

Translocation energy of ions in nano-channels of cell membranes

Sofian Teber*

The Abdus Salam ICTP, Strada Costiera 11, 34014, Trieste, Italy

(Dated: December 2, 2024)

Translocation properties of ionic channels are investigated, on the basis of classical electrostatics, with an emphasis on asymptotic formulas for the potential and field associated with a point charge in the channel. Due to image charges in the membrane, we show that ions in an infinite length channel are anti-confined, *i.e.* subject to a constant repulsive force, with the electrostatic barrier Σ characterized by a “geometric mean” screening $\Sigma \propto e^2/\sqrt{\epsilon_w\epsilon_m}R$ (R being the radius of the pore, and $\epsilon_m \approx 2$ and $\epsilon_w \approx 80$ the room temperature dielectric constants of membrane and water, respectively). There exists a crossover length, $x_0 \propto R\sqrt{\epsilon_w/\epsilon_m} \sim 6.3R$, below which this anti-confinement governs the electrostatics and beyond which the three-dimensional Coulomb potential screened by the membrane takes over. Knowledge of this length enables us to discriminate between long channels, the length L of which satisfies: $L \gg 2x_0$, and short channels for which $L \ll 2x_0$. The latter condition is satisfied by most realistic channels (*e.g.*, gramicidin A where $R \approx 3\text{\AA}$, $L \approx 2.5\text{nm}$ and $2x_0 \approx 3.8\text{nm}$) whose translocation energy is therefore controlled by the part of the self-energy, Σ , arising from the anti-confinement. On this basis, we derive an expression for Σ , with no fitting parameter, which applies to a generic nanochannel of length L and radius R . Our results are related to model-independent translocation properties of nanoscale ionic channels, they improve on previous, curve-fitting, formulas and agree to within 5% with estimates, resulting from numerical simulations, available in the literature on the subject.

I. INTRODUCTION

Even the simplest physical models of bilayer membranes can produce unexpected results, particularly when they concern electrostatic interplays between the membrane and the ionic flow. Consider the phospholipid bilayer as a thin slab of nonconducting material separating two aqueous solutions, and an aqueous ion channel as a cylindrical region connecting the two solutions, see Fig 1. One apparent obstacle to ionic conduction is the electrostatic energy barrier which has to be passed in order to move the ion through the channel. In 1969, Parsegian¹ found that, for an infinite channel, the electrostatic self-energy Σ , *i.e.* the energy required to move an ion from infinity to the center of the channel, is of the order of $16 k_B T$. A major contribution to this self-energy comes from the self-image of the charge due to the consequent difference between the dielectric constant of the water channel ($\epsilon_w \approx 80$, at room temperature) and that of the lipid membrane ($\epsilon_m \approx 2$).

Such a large barrier would prevent *any* ionic flow, contrary to the relatively high conductances observed in experiments². Moreover, these are compatible with barriers not exceeding $6 k_B T$. Subsequent studies focused on mechanisms which would lower the barrier (no screening by counter ions is assumed because typical channel radii are of the order of a few \AA). Taking into account the finite length of the channel (gramicidin A has a characteristic length of 25\AA), as well as a high dielectric shield of the channel, the authors of Refs. 3 and 4 have shown, with the help of numerical methods, a considerable decrease of this barrier, reaching $6.7 k_B T$. A large number of recent studies also address this question, generally focusing on specific models and taking into account of the channel nanostructure, using numerical simulations

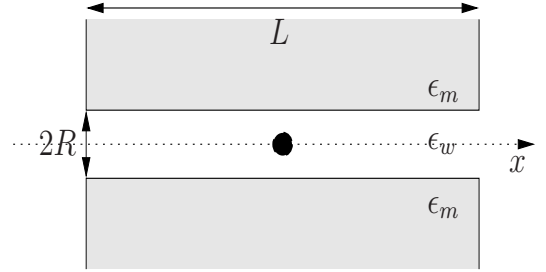


FIG. 1: Schematic view of a channel of length L , radius R with an ion sitting in its center. The channel consists of water, of dielectric constant $\epsilon_w \approx 80$, and is surrounded by the membrane, of dielectric constant $\epsilon_m \approx 2$. A typical channel we are interested in, *e.g.* gramicidin A, has a length $L \approx 2.5\text{nm}$ and a radius $R \approx 3\text{\AA}$.

of the Poisson-Boltzmann or Poisson-Nernst-Planck type, to improve on previous estimates².

In this contribution, the original, model-independent, problem of the electrostatics of point-like ions in an infinite channel is reconsidered, with an emphasis on asymptotic expressions for the potential and field which have not been derived previously. Our quantitative results show the appearance of a length scale: $x_0 \propto R\sqrt{\epsilon_w/\epsilon_m}$, which separates regions, in space, where the effect of the image-charges on the ion at the origin are crucially different. At distances x , along the channel, smaller than x_0 ($x \ll x_0$), the electrostatic potential, φ , is 1D-like and displays an unusual, *i.e.* algebraic in the dielectric constants, screening: $\varphi \propto (e^2/\sqrt{\epsilon_w\epsilon_m}R)(1 - |x|/x_0)$. At distances x , along the channel, larger than x_0 ($x \gg x_0$), the electrostatic potential is 3D-like and everywhere, even in the water channel, screened by the membrane:

$\varphi \propto e^2/\epsilon_m|x|$. In the region $x \ll x_0$, the ions are anti-confined, *i.e.* subject to a constant repulsive force. The crossover length, x_0 , is found to be of the order of, or larger than, the average length of a typical ionic channel and our asymptotic expressions, in the anti-confinement regime, thus capture the essence of the phenomena characteristic of realistic, *i.e.* nano-length, channels. On this physical basis, we will therefore derive a formula for Σ depending on the length L and radius R of a typical pore. This formula for Σ , will be shown to agree, within 5% of accuracy, with the available numerical results in the field and therefore noticeably improves on previous, curve-fitting, expressions. This will lead us to an accurate knowledge, of the main exponential dependence, of the conductance G , of finite-length channels: $G \propto \exp[-\Sigma/k_B T]$.

This article is organized as follows. We first consider the case of an infinite channel where calculations may be carried out straightforwardly. In Sec. II, the electrostatic potential, within the infinite channel, is derived in various asymptotic regimes. The length x_0 is defined. In Sec. III, similar asymptotic formulas for the potential in the membrane are derived. These results are used, in Sec. IV, to derive the components of the electric field and to define, and derive, the anti-confinement force. In Sec. V, the image self-energy of a charge in an infinite channel is derived and the part of this self-energy, arising from the anti-confinement, is singled out. In Sec. VI numerical estimates of the various quantities, derived in the previous sections, are given and compared with exact numerical simulations. In Sec. VII, the case of finite size channels is considered and, on the basis of the results of previous sections, an expression for the self-energy of nano-channels is derived. A comparison is then made with the available results in the literature, based on numerical simulations. Finally, the conclusion is given in Sec. VIII.

II. ELECTROSTATIC POTENTIAL INSIDE AN INFINITE CHANNEL

Consider a point-like ion (charge e) in an infinite cylinder of radius R and of dielectric constant ϵ_w (of water), embedded in a media (the membrane) of dielectric constant $\epsilon_m \ll \epsilon_w$, cf. Fig. 2. The electrostatic potential, $\varphi(x, \mathbf{r}_\perp)$, of such an ion *within* the cylinder is given by:

$$\varphi_{in}(x, \mathbf{r}_\perp) = \int_0^{+\infty} \frac{dk}{\pi} \varphi(k, \mathbf{r}_\perp) \cos(kx), \quad (1)$$

where k is the wavenumber along the (x-)axis of the channel and:

$$\begin{aligned} \varphi_{in}(k, \mathbf{r}_\perp) = & \frac{2e}{\epsilon_w} K_0(kr_\perp) + \\ & \frac{2e}{\epsilon_w} \frac{(\epsilon_w - \epsilon_m) K_0(kR) K_1(kR) I_0(kr_\perp)}{\epsilon_w K_0(kR) I_1(kR) + \epsilon_m K_1(kR) I_0(kR)}, \end{aligned} \quad (2)$$

where I_ν and K_ν are modified Bessel functions of the first and second kind, respectively. The result of Eqs. (1) and (2) may be straightforwardly derived by solving the appropriate inhomogeneous Poisson equation. The first term in Eq. (2) corresponds to the usual ($1/r$ in 3D) Coulomb potential of a charge in an infinite media of dielectric constant ϵ_w and the second term corresponds to the potential due to the image charges (repulsive, as it should be, for $\epsilon_w > \epsilon_m$, because the charge is sitting in the high dielectric constant media). A similar expression has been derived elsewhere⁵ and we shall therefore not prove it here.

At distances smaller than the radius of the channel, $kR \gg 1$, we may use the asymptotic expressions of modified Bessel functions⁶:

$$K_\nu(kR) \approx \frac{\exp(-kR)}{\sqrt{2\pi kR}}, \quad I_\nu(kR) \approx \frac{\exp(kR)}{\sqrt{2kR/\pi}}. \quad (3)$$

Substituting these expressions in the second term, the image part, of Eq. (2), leads to a term $\approx e/\epsilon_w R$, which, at $x \ll R$, is negligible compared to the first one: $e/\epsilon_w|x|$. At distances, $x \ll R$, the images play no role, and the Coulomb potential is the usual 3D one, screened by the dielectric constant of water:

$$\varphi_{in}(\mathbf{r}) = \frac{e}{\epsilon_w r}, \quad r \ll R. \quad (4)$$

Because all phenomena we shall be interested in, in the following, are related to the effect of image charges, R will be our lowest distance cut-off. We will therefore explore the properties of the system at distances larger than the radius of the channel.

We focus on the asymptotics of Eq. (2) at distances, along the channel, larger than its radius, *i.e.* $kR \ll 1$. We will need, in the following, the series expansions of Bessel functions, which may be found in any standard table, *e.g.* Ref. 6. To the highest order of main interest to us, these series expansions read:

$$\begin{aligned} K_0(kR) & \approx \log(2/kR) - \gamma, \\ K_1(kR) & \approx -(\log(2/kR) - \gamma)kR/2, \\ I_0(kR) & \approx 1 + (kR/2)^2 + \dots, \\ I_1(kR) & \approx kR/2 + \dots, \end{aligned} \quad (5)$$

where $\gamma \approx 0.577$ is Euler's constant. With the help of Eq. (5), Eq. (2) may then be approximated by:

$$\begin{aligned} \varphi_{in}(x, \mathbf{r}_\perp) & \approx \frac{e}{\epsilon_w|x|} + \\ & \frac{2e}{\epsilon_m R} \left(1 - \frac{\epsilon_m}{\epsilon_w}\right) \int_0^{+\infty} \frac{d\xi}{\pi} \frac{\xi K_0(\xi) K_1(\xi) \cos(\xi x/R)}{1 + (\xi x_0/R)^2}, \end{aligned} \quad (6)$$

where the dimensionless $\xi = kR$ has been introduced and a characteristic distance, x_0 , appears and reads:

$$x_0 = R \sqrt{\frac{\epsilon_w}{2\epsilon_m} \log(2x_0/R) - \gamma}. \quad (7)$$

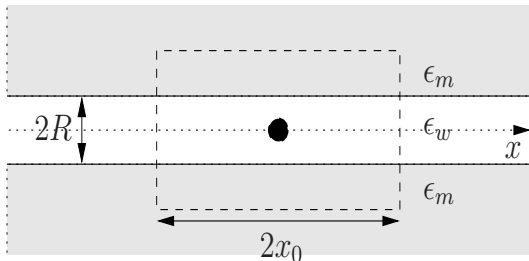


FIG. 2: Schematic view of an infinite channel, including the cylinder of length $2x_0$ and radius x_0 , cf. Eq. (7).

In the limit $\xi \ll R/x_0$, *i.e.* $x \gg x_0$, Eq. (6) reduces to:

$$\varphi(x, \mathbf{r}_\perp = \mathbf{0}) \approx \frac{e}{\epsilon_w |x|} + \frac{2e}{\epsilon_m R} \left(1 - \frac{\epsilon_m}{\epsilon_w}\right) \int_0^{+\infty} \frac{d\xi}{\pi} \xi K_0(\xi) K_1(\xi) \cos(\xi x/R). \quad (8)$$

The integral is a standard one and, as a result:

$$\varphi_{in}(x, \mathbf{r}_\perp) \approx \frac{e}{\epsilon_w |x|} + \frac{e}{\epsilon_m |x|} \left(1 - \frac{\epsilon_m}{\epsilon_w}\right) = \frac{e}{\epsilon_m |x|}, \quad x \gg x_0, \quad r_\perp < R, \quad (9)$$

which corresponds to the usual 3D Coulomb interaction screened by the membrane.

In the limit $\xi \gg R/x_0$, *i.e.* $R \ll x \ll x_0$, Eq. (6) reads:

$$\varphi_{in}(x, \mathbf{r}_\perp) = \frac{e}{\epsilon_m x_0} K_0(R/x_0) J_0(r_\perp/x_0) \exp(-|x|/x_0), \quad R \ll x \ll x_0, \quad r_\perp < R, \quad (10)$$

where corrections in x/x_0 , r_\perp/x_0 as well as R/x_0 have been summed, to all orders, into the special functions appearing in Eq. (10). With the help of series expansions of these special functions, to the lowest orders in the small quantities above: $J_0(r_\perp/x_0) \approx 1$ and: $K_0(r_\perp/x_0) \approx -\gamma + \log(2x_0/R)$, Eq. (10) yields:

$$\varphi_{in}(x, \mathbf{r}_\perp) \approx \frac{e}{\epsilon_m x_0} (\log(2x_0/R) - \gamma) \left(1 - \frac{|x|}{x_0}\right), \quad R \ll x \ll x_0, \quad r_\perp < R. \quad (11)$$

Eq. (11) shows that the potential is 1D-like, because of the linear dependence on the coordinate, x , along the channel.

III. ELECTROSTATIC POTENTIAL OUTSIDE THE INFINITE CHANNEL

In this section, we will still focus on the ion *within* the pore but determine the potential due to this ion *outside* the pore, *i.e.* for $r_\perp > R$. This potential reads:

$$\varphi_{out}(k, \mathbf{r}_\perp) = \frac{2e}{kR \epsilon_w K_0(kR) I_1(kR) + \epsilon_m K_1(kR) I_0(kR)} K_0(kr_\perp) \quad (12)$$

Being interested in distances, along the axis of the pore, which are larger than R , *i.e.* $kR \ll 1$, Eq. (12) reads, in this limit:

$$\varphi_{out}(x, \mathbf{r}_\perp) = \frac{2e}{\epsilon_m x_0} \int_0^{+\infty} \frac{d\xi}{\pi} \frac{K_0(\xi r_\perp/x_0) \cos(\xi x/x_0)}{1 + \xi^2} \quad (13)$$

where the dimensionless variable $\xi = kx_0$ and x_0 is given by Eq. (7).

For $x \gg x_0$, we recover the potential of a 3D point-like charge:

$$\varphi_{out}(x, \mathbf{r}_\perp) = \frac{e}{\epsilon_m r}, \quad x \gg x_0, \quad \forall r_\perp > R, \quad (14)$$

where $r = \sqrt{x^2 + r_\perp^2}$ and the screening is by the dielectric constant of the membrane.

For $x \ll x_0$, the potential reads:

$$\varphi_{out}(x, \mathbf{r}_\perp) = \frac{e}{\epsilon_m x_0} \frac{\pi}{2} [H_0(r_\perp/x_0) - Y_0(r_\perp/x_0)], \quad x \ll x_0, \quad r_\perp > R, \quad (15)$$

where H_0 is a Struve function and Y_0 is a Neumann function. Using asymptotic and series representations of these special functions⁶, we find that:

$$\varphi_{out}(x, \mathbf{r}_\perp) \approx \frac{e}{\epsilon_m x_0} [\log(2x_0/r_\perp) - \gamma], \quad x \ll x_0, \quad R < r_\perp \ll x_0, \quad (16)$$

and that:

$$\varphi_{out}(x, \mathbf{r}_\perp) = \frac{e}{\epsilon_m r_\perp}, \quad x \ll x_0, \quad r_\perp \gg x_0. \quad (17)$$

Eq. (16) shows that, inside the shell of radius x_0 outside the pore, the potential is 2D-like. As for the 1D potential of Eq. (11), this implies that field lines are mostly located within the water channel because of its high dielectric constant. Beyond x_0 , such a potential crosses over to the 3D Coulomb potential of Eq. (17), similarly to what happens inside the channel, cf. Eq. (9).

The potential outside the pore of Eq. (16) has also an x -dependence which we have neglected as a first approximation. Taking this dependence into account, the latter may formally be expressed as:

$$\varphi_{out}(x, \mathbf{r}_\perp) = \frac{e}{\epsilon_m x_0} K_0(r_\perp/x_0) \exp(-|x|/x_0), \quad x \ll x_0, \quad R < r_\perp \ll x_0. \quad (18)$$

The series expansions of the special functions appearing in Eq. (18), give the dominant contributions in the small parameters x/x_0 and r_\perp/x_0 , *e.g.* the exponential gives the linear dependence on $|x|$ and the MacDonald function K_0 gives the logarithmic dependence on r_\perp .

IV. ELECTRIC FIELD AND ANTI-CONFINEMENT FORCE IN AN INFINITE CHANNEL

The previous sections have shown the importance of the crossover length, x_0 , which separates regions, in

space, characterized by different sectors of the electrostatic potential controlled by the effect of image charges. We proceed now on deriving the corresponding components of the electric field and define the anti-confinement of the ions in the channel.

Within the channel and at distances, from the ion at the origin, smaller than x_0 , cf. Fig. 2, the electrostatic potential is given by Eq. (10), which corresponds, in the first order in x/x_0 to a 1D Coulomb potential, cf. Eq. (11). The corresponding components of the electric field then formally (expansions of the various functions involved have to be taken) read:

$$E_x^{in} = \frac{e}{\epsilon_m x_0^2} K_0(R/x_0) J_0(r_\perp/x_0) \exp(-|x|/x_0),$$

$$R \ll x \ll x_0, \quad r_\perp < R, \quad (19)$$

$$E_\perp^{in} = \frac{e}{\epsilon_m x_0^2} K_0(R/x_0) J_1(r_\perp/x_0) \exp(-|x|/x_0),$$

$$R \ll x \ll x_0, \quad r_\perp < R. \quad (20)$$

These expressions display the role of the image force: J_0 is unity at the origin, so the longitudinal field is constant, non-zero and positive, which implies the *anticonfinement* of the ions in the channel. On the other hand, J_1 vanishes at the origin, so there is no component of transverse force on the charge. The anti-confinement force, which strongly prevents more than one ion to be inside the pore, therefore reads:

$$F_a = eE_x^{in}(x = r_\perp = 0) = \frac{e^2}{\epsilon_m x_0^2} (\log(2x_0/R) - \gamma). \quad (21)$$

Another particular sector, of the electrostatic potential, corresponds to the cylindrical shell surrounding the pore, at $R \ll r_\perp \ll x_0$, still within the distance x_0 along the channel, from the origin. In this region, Eq. (16) shows that the potential is 2D-like. With the help of Eq. (18), which includes higher order corrections, the corresponding components of the electric field then formally read:

$$E_x^{out} = \frac{e}{\epsilon_m x_0^2} K_0(r_\perp/x_0) \exp(-|x|/x_0),$$

$$R \ll x \ll x_0, \quad R < r_\perp \ll x_0, \quad (22)$$

$$E_\perp^{out} = \frac{e}{\epsilon_m x_0^2} K_1(r_\perp/x_0) \exp(-|x|/x_0),$$

$$R \ll x \ll x_0, \quad R < r_\perp \ll x_0. \quad (23)$$

Finally, the last sector corresponds to the region outside the cylinder of radius x_0 and length $2x_0$ where the potential is 3D-like and isotropic (cf. Eqs. (9), (14) and (17)). This potential is still unusual, within the water channel, because, due to the effect of image charges, it is screened by the membrane only: $\varphi_{out}(\mathbf{r}) = e/\epsilon_m r$, ($x > x_0, \forall r_\perp$), ($r_\perp > x_0, \forall x$). The electric field then corresponds to the usual 3D electric field screened by the

dielectric constant of the membrane. We denote this field by:

$$E^{ext} = \frac{e}{\epsilon_m r^2}$$

$$(x > x_0, \forall r_\perp), (r_\perp > x_0, \forall x). \quad (24)$$

V. IMAGE SELF-ENERGY OF AN ION IN AN INFINITE CHANNEL

The total self-energy of a charge in the channel may be derived, with the help of the self-potential, by the identity:

$$\Sigma^{(\infty)} = \frac{e}{2} \varphi(0). \quad (25)$$

where the upper script (∞) , refers to the fact that an infinite channel is considered. As for the electrostatic potential, in Eq. (25), we consider the self-energy arising due to image charges, the *image self-energy*, and measure it with respect to the Born energy of the charge $e^2/2\epsilon_w a$, where a is the radius of the charge. As for the electrostatic potential, we decompose this image self-energy, by considering a part, Σ_a , arising from the region $x \ll x_0$, and a part related to larger distances, $\Sigma_{ext}^{(\infty)}$, where the potential is the regular 3D-like (but screened everywhere by the membrane). Hence:

$$\Sigma^{(\infty)} = \Sigma_a^{(\infty)} + \Sigma_{ext}^{(\infty)}. \quad (26)$$

We focus first on the part arising from the anti-confinement, $\Sigma_a^{(\infty)}$. Suppose that the charge is brought to the origin along the channel. The corresponding self-potential is given by Eq. (10) at $x = 0$ and $r_\perp = 0$. The corresponding self-energy then reads:

$$\Sigma_a^{(\infty)} \approx \frac{1}{2} \frac{e^2}{\epsilon_m x_0} (\log(2x_0/R) - \gamma). \quad (27)$$

This AC self-energy may be evaluated by a similar way by considering that the charge has been brought to the origin from the membrane (*i.e.* perpendicular to the pore). Then, Eq. (18) has to be used for the self-potential which brings us back to Eq. (27).

In order to determine the total image self-energy, and compare it with exact numerical results, we need to take care of boundary terms, arising from the cylindrical geometry of the system and which influence the final value of the self-energy. We find it therefore convenient to re-express Eq. (25) in the form:

$$\Sigma^{(\infty)} = \frac{1}{2} e \int d\mathcal{V} \rho(\mathbf{r}) \varphi(\mathbf{r}), \quad \rho(\mathbf{r}) = \delta(\mathbf{r}), \quad (28)$$

where \mathcal{V} is the total volume of the system. Using the inhomogeneous Poisson equation, we may express the density of test charge as a function of the potential, in Eq. (28), to obtain:

$$\Sigma = \frac{1}{8\pi} \int d\mathcal{V} \epsilon(\mathbf{r}) (\nabla \varphi(\mathbf{r}))^2. \quad (29)$$

We focus first on contributions to the image self-energy, within x_0 :

$$\Sigma_a^{(\infty)} = \frac{\epsilon_w}{8\pi} \int_{in} d\mathcal{V}(\mathbf{E}^{in})^2 + \frac{\epsilon_m}{8\pi} \int_{out} d\mathcal{V}(\mathbf{E}^{out})^2. \quad (30)$$

The first term in Eq. (30), is associated with the electric field inside the cylinder, cf. Eqs. (19) and (20), and reads:

$$\Sigma_{a,in}^{(\infty)} = \frac{\epsilon_w e^2}{4\epsilon_m^2 x_0} K_0^2\left(\frac{R}{x_0}\right) \int_0^{\frac{R}{x_0}} d\xi_{\perp} \xi_{\perp} [J_0^2(\xi_{\perp}) + J_1^2(\xi_{\perp})] \quad (31)$$

where $\xi_{\perp} = r_{\perp}/x_0$. Expanding the integral in R/x_0 leads, in the lowest order in R/x_0 , to:

$$\Sigma_{a,in}^{(\infty)} = \frac{1}{2} \frac{\epsilon_w e^2 R^2}{4\epsilon_m^2 x_0^3} K_0^2(R/x_0), \quad (32)$$

where higher order terms in R/x_0 are neglected. Finally, using Eq. (7), yields:

$$\Sigma_{a,in}^{(\infty)} = \frac{1}{4} \frac{e^2}{\epsilon_m x_0} (\log(2x_0/R) - \gamma), \quad (33)$$

With the same notations, the second term, in Eq. (30), originates from the electric field within x_0 but outside the cylinder, cf. Eqs. (22) and (23), and reads:

$$\Sigma_{a,out}^{(\infty)} = \frac{e^2}{4\epsilon_m x_0} \int_{R/x_0}^1 d\xi_{\perp} \xi_{\perp} [K_0^2(\xi) + K_1^2(\xi)]. \quad (34)$$

In the lowest order in R/x_0 , the result is:

$$\Sigma_{a,out}^{(\infty)} = \Sigma_{a,in}^{(\infty)} - 0.13 \frac{e^2}{2\epsilon_m x_0}, \quad (35)$$

where the second term is a boundary correction, due to the cylindrical geometry. Including this boundary correction, the image self-energy, in the lowest order in R/x_0 , reads:

$$\Sigma_a^{(\infty)} = \frac{1}{2} \frac{e^2}{\epsilon_m x_0} (\log(2x_0/R) - \gamma) - 0.13 \frac{e^2}{2\epsilon_m x_0}, \quad (36)$$

where the first term returns us back to Eq. (27).

We now proceed to determine the part of the self-energy, $\Sigma_{ext}^{(\infty)}$, at distances $x \gg x_0$. This reads:

$$\Sigma_{ext}^{(\infty)} = \frac{\epsilon_m}{8\pi} \int_{ext} d\mathcal{V}(\mathbf{E}^{ext})^2, \quad (37)$$

where the external volume is beyond the cylinder of length $2x_0$ and radius x_0 . With the help of Eq. (24), this reads:

$$\Sigma_{ext}^{(\infty)} = \frac{\pi}{8} \frac{e^2}{2\epsilon_m x_0}, \quad (38)$$

and should be contrasted with the naive expression: $\Sigma_{ext}^{(\infty)} = e^2/2\epsilon_m x_0$, based on a spherical symmetry.

From Eqs. (36) and (38), the total image self-energy, Eq. (26), to the lowest order in R/x_0 , reads:

$$\Sigma^{(\infty)} = \frac{1}{2} \frac{e^2}{\epsilon_m x_0} (\log(2x_0/R) - \gamma) + 0.26 \frac{e^2}{2\epsilon_m x_0}. \quad (39)$$

It should be noticed that in all previous derivations, only the lowest order term, in R/x_0 , has been taken into account. Higher order terms would lower the energy. We therefore overestimate the energy. The agreement will, however, remain excellent with respect to numerical simulations, in this approximation, as we proceed to prove in the next section.

VI. NUMERICAL ESTIMATES FOR THE INFINITE CHANNEL

The most straightforward and accurate way, of determining the value of the self-energy of an ion, Eq. (25), has been taken by Parsegian who has used a formula⁵, similar to Eqs. (1) and (2), which has been substituted in Eq. (25), and evaluated numerically. With the help of our Eqs. (1) and (2), Eq. (25) reads:

$$\Sigma^{(\infty)} = \int_0^{+\infty} \frac{dk}{\pi} \frac{e^2}{\epsilon_w \epsilon_m} \frac{(\epsilon_w - \epsilon_m) K_0(kR) K_1(kR)}{\epsilon_w K_0(kR) I_1(kR) + \epsilon_m K_1(kR) I_0(kR)} \quad (40)$$

where the energy is measured with respect to the Born energy, and may be evaluated with any standard software. We shall refer to this solution, for the image self-energy, as the *exact numerical solution*.

Our analysis of the previous sections, on the other hand, has revealed some important features of the electrostatics of ion channels, in particular the crossover length x_0 , the concept of anti-confinement and expressions for all quantities of interest, including the self-energy of Eq. (40) and the main contribution to this image self-energy, the anti-confinement part. We proceed to evaluate these expressions, by taking the case of, *e.g.* the model-pore gramicidin A which has a radius $R = 3.0\text{\AA}$ and a length $L = 25.0\text{\AA}$, and for the typical room-temperature values: $\epsilon_m = 2$ and $\epsilon_w = 80$.

The crossover length, x_0 , has to be determined self-consistently from Eq. (7). In the logarithmic approximation, this length reads:

$$x_0 \approx R \sqrt{\frac{\epsilon_w}{2\epsilon_m}} \sqrt{0.5 \log(2\epsilon_w/\epsilon_m) - \gamma}. \quad (41)$$

Using a more precise graphical method yields:

$$x_0 \approx 6.3R, \quad (42)$$

where we have used the fact that $\epsilon_m = 2$ and $\epsilon_w = 80$. In the case of the model-pore gramicidin A ($R = 3.0\text{\AA}$): $x_0 \approx 19.0\text{\AA}$. The peculiar potential of Eq. (11) plays a dominant role over this length, from the origin. Beyond the length x_0 , the confinement potential crosses over to

TABLE I: Image self-energy, of an ion in an infinite channel, in various units from the exact numerical calculation, see Eqs. (1), (2) and discussion below them as well as Ref. 1, and from our asymptotic formulas, Eq. (39). We have taken $\epsilon_m = 2$ and $\epsilon_w = 80$.

Self-energy unit	Exact	Eq. (39)
$e^2/\sqrt{\epsilon_w\epsilon_m}R$	1.08	1.11
$e^2/\epsilon_m R$	0.17	0.17
$e^2/\epsilon_w R$	6.80	7.01
$k_B T$	16.0	16.6

$(R = 3.0\text{\AA})$

the 3D Coulomb potential. We have therefore to compare the length of the channel, $L = 25.0\text{\AA}$, to the region where the anti-confinement dominates: $2x_0 \approx 38.0\text{\AA}$.

Obviously, such a value of $2x_0 > L$ shows that the anti-confinement of the ions dominates in the model nanopore. We shall come back on this crucial fact, in the next section, when dealing with finite-size effects. Substituting the expression of x_0 , in Eq. (10), leads to:

$$\varphi_{in}(x) \approx \frac{e}{\sqrt{\epsilon_w\epsilon_m}R} \sqrt{2(\log(2x_0/R) - \gamma)} \exp(-|x|/x_0),$$

$$R \ll x \ll x_0 \quad (43)$$

which displays the "geometric mean" screening: $\propto \sqrt{\epsilon_w\epsilon_m}$, and is affected by a logarithmic factor characteristic of the intrinsic 1D nature of the system (see also Ref. 7 where the geometric-like screening has been considered qualitatively).

As a consequence of Eq. (43), if an ion is in the pore, any additional ion will feel a constant repulsive force, *i.e.* an anti-confinement force, cf. Eq. (21). Substituting the expression of x_0 , cf. Eq. (7), in Eq. (21), this force simply reduces to:

$$F_a = \frac{2e^2}{\epsilon_w R^2}. \quad (44)$$

This is an unrealistically large (because we consider an infinite channel) force: $F_a \approx 48.9 \text{ eV/\AA}$. The strong repulsion originating from Eq. (44) is therefore responsible for the large image self-energy of the charge, cf. Eq. (27), which, with the help of Eq. (7), and to the lowest order in R/x_0 , reads:

$$\Sigma_a^{(\infty)} = \frac{1}{2} \frac{e^2}{\sqrt{\epsilon_w\epsilon_m}R} \sqrt{2(\log(2x_0/R) - \gamma)} - C_g, \quad (45)$$

where $C_g = 0.13(e^2/2\epsilon_m x_0)$, is the geometric correction, appearing in Eq. (36). With the help of $\epsilon_m = 2$ and $\epsilon_w = 80$, Eq. (45) yields:

$$\Sigma_a^{(\infty)} \approx (44.02/R - 2.90/R)k_B T \approx (41.12/R)k_B T, \quad (46)$$

where $C_g \approx (2.90/R)k_B T$. This correction is not negligible when it comes to compare our results with precise numerical estimates. For $R = 3\text{\AA}$, $C_g \approx 0.97k_B T$, and

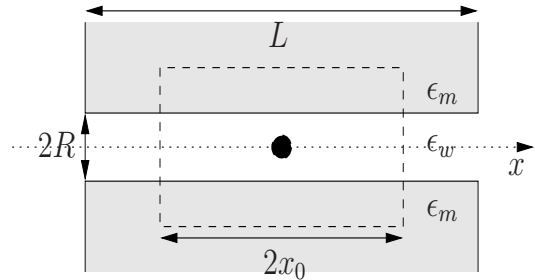


FIG. 3: Schematic view of a long channel, for which: $L \gg 2x_0$, cf. Eq. (7).

this yields: $\Sigma_a^{(\infty)} \approx 13.7k_B T$. For $R = 2\text{\AA}$, a drastic increase results: $\Sigma_a^{(\infty)} \approx 20.56k_B T$, where $C_g \approx 1.45k_B T$. On the other hand, for $R = 5\text{\AA}$, this quantity is reduced to: $\Sigma_a^{(\infty)} \approx 8.22k_B T$, $C_g \approx 0.58k_B T$.

To estimate the total image self-energy one should consider Eq. (39), which takes into account of the large-distance part of the energy. Adding this contribution, to Eq. (46), yields:

$$\Sigma^{(\infty)} \approx (49.82/R)k_B T. \quad (47)$$

For $R = 3\text{\AA}$, Eq. (47), yields: $\Sigma^{(\infty)} \approx 16.6k_B T$. Numerical estimates for $\Sigma^{(\infty)}$, in various units, are displayed in Tab. I. They agree with the exact results of numerical simulations.

Notice that, to express the self-energy in units of $k_B T$, where k_B is Boltzmann's constant, we have found it convenient to introduce Bjerrum's length, l_B . At room temperature and in water, Bjerrum's length reads: $l_B = e^2/\epsilon_w k_B T$. To be able to compare safely our results with previous studies^{3,4} we take the value $l_B \approx 7.038\text{\AA}$ (Jordan converts the values of Levitt (in $k_B T$) in units of $e/\epsilon_w R$ and this value of l_B agrees with the conversion).

VII. FINITE-SIZE EFFECTS: ANTI-CONFINEMENT AND TRANSLOCATION ENERGY IN NANO-CHANNELS

In the case of a finite-length channel, calculations similar to the infinite length case lead to coupled non-linear integral equations, at the level of the boundary conditions imposed on the electrostatic potential of the inhomogeneous Poisson equation. Even an approximate solution of these boundary equations seems untractable, analytically, and numerical simulations appear to be necessary. Such a numerical task has been undertaken in Refs. 3 and 4, by two different numerical methods, showing that the self-energy $\Sigma^{(\infty)}$ becomes of the order of $\Sigma^{(L)} \approx 6.7k_B T$ for a length $L = 25.0\text{\AA}$ and a radius $R = 3\text{\AA}$. Two formulas were also proposed to take into account of the finite size effects. For large lengths

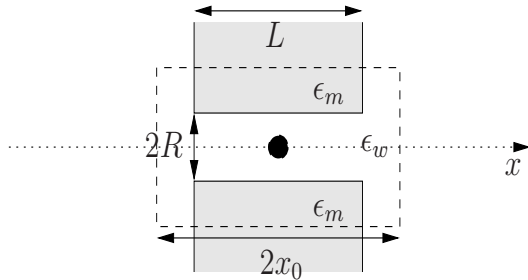


FIG. 4: Schematic view of a nano-length channel, for which: $L \ll 2x_0$, cf. Eq. (7). This case corresponds to the typical channels we are interested in, *e.g.* gramicidin A for which $L \approx 2.5\text{nm}$, $R \approx 3\text{\AA}$ and $2x_0 \approx 12.6R \approx 3.8\text{nm}$.

Parsegian has proposed³:

$$\Sigma^{(L)} \approx \Sigma^{(\infty)} - \frac{e^2}{\epsilon_m L} \log\left(\frac{2\epsilon_w}{\epsilon_m + \epsilon_w}\right), \quad (48)$$

where the first term is the self-energy of the infinite channel and the second term corresponds to the self-energy of a charge in a membrane without a pore. On the light of the previous sections, this "large length" ansatz, should work for lengths larger than $2x_0$. We may understand this result on the basis of Fig. 3, by decomposing the self-energy into two parts, while bringing the charge from infinity to the origin:

$$\Sigma^{(L)} \approx \Sigma_a^{(\infty)} + \frac{e^2}{2\epsilon_m} \left(\frac{1}{x_0} - \frac{2}{L}\right), \quad (49)$$

where the first term corresponds to the anticonfinement part of the self-energy of the infinite channel and the second, to the energy required to displace the charge from $L/2$ to x_0 (for the finite channel image charges do not play any role beyond $L/2$ from the origin and the corresponding self-energy contribution has been neglected). Up to numerical coefficients, the first two terms yield $\Sigma^{(\infty)}$ and the last term yields the (reducing) effect of the membrane. Unfortunately, Eq. (48) seems to work only for unrealistically long channels, well beyond $2x_0$, *i.e.* the percentage of error, with respect to numerical simulations, becomes less than 5% for lengths larger than $40R$.

For the most relevant case of small length channels, cf. Fig. 4, Jordan has proposed, without any justification other than curve-fitting, the following expression⁴:

$$\Sigma^{(L)} \approx \Sigma^{(\infty)} [1 - \exp(-b\delta)], \quad (50)$$

where $b = 0.131$ and δ is the reduced channel length, $\delta = L/2R$. We see immediately that the characteristic length appearing in the exponential corresponds to: $L_0 \approx 2.44x_0$. The "small-length" case will therefore obviously correspond to the regime where $L \ll 2x_0$. We now proceed to justify the curve-fitting Eq. (50) and improve on the result of Jordan.

As is clear from the previous lines, the knowledge of x_0 allows us to consider that channels of characteristic length: $L \ll 2x_0$, are finite, with respect to the anti-confinement (AC) part of the self-energy, whereas channels of characteristic lengths: $L \gg 2x_0$, are formally infinite with respect to the same quantity. As a matter of fact, the AC self-energy of a channel of length $L \gg 2x_0$ saturates: $\Sigma_a^{(L)} \approx \Sigma_a^{(\infty)}$. On the other hand, the AC self-energy of a channel of length $L \ll 2x_0$, is determined with the help of Eq. (43), as: $\Sigma^{(L)} = (e/2)(\varphi_{in}(0) - \varphi_{in}(L/2))$. The first term corresponds to $\Sigma_a^{(\infty)}$ and the second gives the leading correction in L/x_0 . Actually, higher order corrections in $L/2x_0$ are important. As in Eq. (43), such corrections may be resummed in an exponential factor. This yields:

$$\Sigma_a^{(L)} \approx \Sigma_a^{(\infty)} [1 - \exp(-L/2x_0)], \quad L \ll 2x_0, \quad (51)$$

where $\Sigma_a^{(\infty)}$ is given by Eq. (45), which justifies the functional form of Jordan's expression on a physical basis. In the lowest order in $L/2x_0$, $\Sigma_a^{(L)}$, in Eq. (51), increases linearly with L , a feature of the anti-confinement: $\Sigma_a^{(L)} \approx \Sigma_a^{(\infty)} L/2x_0$. For the case of interest ($\epsilon_m = 2$ and $\epsilon_w = 80$), the image self-energy of a channel of length L and radius R reads:

$$\Sigma_a^{(L)}(L, R) \approx \left(\frac{44.02}{R} - C_g\right) [1 - \exp[-\delta/6.3]] k_B T, \quad L \ll 2x_0, \quad (52)$$

where $\delta = L/2R$ and $C_g \approx (2.90/R)k_B T$ from the previous section. Actually, Eq. (52) works better than Eq. (48) at lengths $L \approx 2x_0$. This implies that, in Eq. (48), corrections due to the presence of the membrane beyond the region of confinement, $|x| > x_0$, manifest only for very large lengths, $L \gg 2x_0$, which is beyond the lengths of the channels we are interested in.

We also notice from Eq. (52), that the self-energy cannot be expressed in terms of a single scaling parameter, here $\delta = L/2R$. Eq. (52) depends separately on L and R . This fact is very clear from the work of Levitt, that we have reproduced in Tab. II. For a given parameter δ , *e.g.* $\delta = 6.25$, the channel ($L = 25\text{\AA}$, $R = 2\text{\AA}$) is characterized by $\Sigma^{(L)} \approx 13.3k_B T$ whereas the channel ($L = 37.5\text{\AA}$, $R = 3\text{\AA}$) is characterized by: $\Sigma^{(L)} \approx 8.91k_B T$. This is a drastic energy variation, which is well reproduced by Eq. (52).

Eq. (52) gives therefore a fit-parameter free expression for the self-energy of a charge in nano-channels, in the range of validity: $R \ll L \ll 2x_0$. As can be seen from Tab. II, the average percentage of error (in the regime of validity) of Eq. (52), with respect to numerical simulations, is: 2.16% for the data of column DL and PJ1 and of 4.14% for column PJ2. With respect to the data of Levitt³ we are within 3.% of error and with respect to the data of Jordan⁴ within 5.%, *i.e.* similar than the error bar of Jordan's curve-fitting formula. Notice also that the accuracy extends beyond $L = 2x_0$ (or $\delta = \delta_0 = 6.3$), with an error still within 3.%, with respect to PJ1 and

within 6.%, with respect to PJ2. In the limit $L \gg 2x_0$, Eq. (52) also gives a better accuracy than Eq. (48) the values of which have been displayed in the last column of Tab. II. Better accuracy, with respect to the numerical simulations, may be reached if C_g is considered as a fitting parameter but we shall not dwell on this point as our fit-free results have already a very good accuracy.

VIII. CONCLUSION

In summary, we have shown that finite- T transport, across ionic channels, is determined by zero-temperature (as there is no screening by counterions within the channels we are interested in) classical electrostatics. Our main result is an expression for the image self-energy of a finite nanochannel, Eqs. (51) and (45), with no fitting parameter and an agreement within an error of 5% with the existing numerical simulations available from the literature on the subject. Combining Eqs. (51) and (45) the most general expression for the image self-energy of a channel of length L and radius R reads:

$$\Sigma_a^{(L)}(L, R) = \frac{\mathcal{N}}{2} \frac{e^2}{\sqrt{\epsilon_w \epsilon_m} R} \sqrt{2(\log(2x_0/R) - \gamma)[1 - \exp(-L/2x_0)]},$$

$$R \ll L \ll 2x_0, \quad (53)$$

where $\gamma \approx 0.577$ is Euler's constant, x_0 is determined by Eq. (7) and $\mathcal{N} = 1 - 0.13$, is a numerical coefficient originating from C_g , cf. Eq. (45). The latter may be of the order of a few $k_B T$ (depending on the characteristics of the channel under consideration) and has to be taken into account for numerical estimates. In the lowest order in $L/2x_0$, Eq. (53) increases linearly with the length of the channel, a feature of the anti-confinement of ions in nanoscale channels.

The image self-energy of Eq. (53) corresponds to the *translocation*, or activation, energy through a finite length channel, *e.g.* the energy required to displace a charge from the entrance of a channel to its center. In relation with experiments, the existence of such electrostatic barrier requires a threshold voltage difference,

$e\Delta V_c(L, R) = \Sigma_a^{(L)}(L, R)$ (where the self-energy is in units of eV), across the channel in order to pass an ion through it (no chemical potential difference is taken into account here). Equivalently, this corresponds to the existence of a threshold electric field: $E_c = \Delta V_c(L, R)/L$, applied along the length of the channel. As an inverse problem, measurement of this threshold field would then give access to information on the channel, its radius or length, with the help of Eq. (53).

The image self-energy of Eq. (53) determines the main exponential dependence of the conductance of a nanoscale channel:

$$G \propto \exp[-\Sigma_a^{(L)}(L, R)/k_B T]. \quad (54)$$

Up to now, all our estimations were performed at room temperatures for $\epsilon_w = 80$. Actually, the dielectric constant of water is sensitive to temperature and varies from $\epsilon_w(273 K) = 87.78$ to $\epsilon_w(323 K) = 69.91$. Basic estimations of $\Sigma_a \equiv \Sigma_a(T)$ which take into account of this temperature variation of ϵ_w show that the ratio $\Sigma_a(T)/k_B T$ becomes approximately temperature - independent (the coefficient C_T defined as: $\Sigma_a(T)/T|_{T=273K} = C_T \Sigma_a(T)/T|_{T=323K}$ is equal to $C_T \approx 1.18$ for a temperature-independent dielectric constant and to $C_T \approx 1.00$ with the above temperature-dependence of ϵ_w). This implies that, despite the fact that the conductance is affected by an exponentially small factor, its thermal dependence is weak so that the ionic flow through channels of cell membranes is stable, being approximately constant over more than two decades of units of temperature, around room temperature.

Acknowledgments

I am grateful to B. I. Shklovskii for fruitful discussions which initiated this work. I thank A. V. Finkelstein, D. N. Ivankov and A. M. Dykhne for sharing their version of the expression of the image self-energy for the infinite channel case, cf. Ref. 8. I also thank G. Huber for general comments on the manuscript. This work is supported by INTAS Grant No. 2212.

* Electronic address: steber@ictp.trieste.it

¹ Parsegian A, 1969 *Nature* **221**, March 1, 844.

² Hille B, Ionic Channels of Excitable Membranes, Sinauer Associates; 3rd Casebound edition (July 1, 2001).

³ Levitt D G, 1978 *Biophys. J.* **22** 209.

⁴ Jordan P C, 1982 *Biophys. J.* **39** 157.

⁵ Smythe W R, Static and Dynamic Electricity (International Series in Pure and Applied Physics), McGraw-Hill Companies (January 1968).

⁶ Gradshteyn I S and al, Table of Integrals, series and products, Academic Press; 6 edition (July 31, 2000).

⁷ Finkelstein A V and Ptitsyn O B, Protein Physics (chapter 12), Academic Press, An Imprint of Elsevier Science; Amsterdam (2002).

⁸ Finkelstein A V, Ivankov D N and Dykhne A M (in preparation).

TABLE II: Image self-energy of an ion in a channel of length L , in units of $k_B T$, as a function of the reduced channel length $\delta = L/2R$, where R is the radius of the channel. We have taken $\epsilon_m = 2$ and $\epsilon_w = 80$. Energies are in units of $k_B T$ and lengths are in units of Å. The crossover length, $L_0 = 2x_0$ between large and small channels, corresponds to the universal value (independent of the length and radius of the channel): $\delta_0 = 6.3$. Our asymptotic calculations are valid for lengths: $R < L < 2x_0$. Eq. (52), is taken with no fitting parameter. The percentage of error appearing in columns DL, PJ1 and PJ2, is that of Eq. (52) with respect to the numerical simulations.

L	R	δ	DL ^a	PJ1 ^b	PJ2 ^c	Eq. (52)	Eq. (48)
9	3	1.5	-	2.58 (11.0%)	2.51 (13.4%)	2.90	-
15	3	2.5	4.34 (3.3%)	-	4.28 (4.7%)	4.49	3.45
21	3	3.5	-	5.86 (0.3%)	5.82 (0.3%)	5.84	7.04
25	3	4.17	6.72 (1.4%)	-	-	6.63	8.47
30	3	5.	-	7.69 (2.4%)	7.72 (2.8%)	7.51	9.73
35	3	5.83	8.48 (2.5%)	-	-	8.27	10.62
37.5	3	6.25	-	8.91 (3.4%)	9.00 (4.4%)	8.62	10.98
50	3	8.33	10.25 (2.0%)	-	10.59 (5.4%)	10.05	12.24
52.5	3	8.75	-	10.45 (1.6%)	10.87 (5.6%)	10.29	12.42
75	3	12.5	-	11.53 (2.5%)	12.50 (5.8%)	11.82	13.49
∞	3	∞	16	-	-	14.70	16
15	2	3.75	9.3 (0.1%)	-	-	9.22	-
25	2	6.25	13.3 (2.8%)	-	-	12.94	-
35	2	8.75	15.6 (0.1%)	-	-	15.43	-
50	2	12.5	17.2 (3.0%)	-	-	17.73	-
∞	2	∞	24	-	-	20.56	-
15	5	1.5	1.54 (11.5%)	-	-	1.74	-
25	5	2.5	2.59 (3.7%)	-	-	2.69	-
35	5	3.5	3.50 (0.3%)	-	-	3.51	-
50	5	5	4.59 (1.8%)	-	-	4.51	-
∞	5	∞	9.62	-	-	8.22	-

^aAs determined from Table I of Levitt³.

^bAs determined from Table I, column 2, of Jordan⁴.

^cAs determined from Table I, column 3, of Jordan⁴.